# Supplementary information

## I. MODEL OF BIOFILM DEVELOPMENT IN THE NETWORK

*Flow* Flow is modeled using analytical solutions within each channel of the network of connected channels. For any channel connecting nodes $\alpha$ and $\beta$, we have a Darcy-type relationship in the form

$$P^\star_{\alpha\beta} = R^\star\left(\phi_{\alpha\beta}\right) Q^\star_{\alpha\beta}, \tag{1}$$

with

- $P^\star_{\alpha\beta} = P^\star_\alpha - P^\star_\beta$ the pressure difference between nodes $\alpha$ and $\beta$,
- $Q^\star_{\alpha\beta}$ the flow rate in the channel,
- $R^\star\left(\phi_{\alpha\beta}\right)$ is the hydraulic resistance of the channel.

Hydraulic resistance is a function of the volume fraction occupied by the biofilm in the channel, $\phi_{\alpha\beta}$, and defined as $R^\star\left(\phi_{\alpha\beta}\right) = R^\star_0\left(1-\phi_{\alpha\beta}\right)^{-2}$. $R^\star_0$ is the resistance of the empty channel and defined as $R^\star_0 = A\mu L h^{-4}$ with $\mu$ the viscosity of the fluid, $L$ the length of each edge, $h$ the width of the channel and $A = \frac{12}{1-\sum_{n,\text{odd}}^{\infty}\frac{1}{n^5}\frac{192}{\pi^5}\tanh\left(n\frac{\pi}{2}\right)}$ in the case of square cross-sections, which is often approximated as $A = \frac{12}{1-0.917\times 0.63}$ Bruus [1].

Mass conservation at node $\alpha$ reads $\sum_{\beta\in\mathcal{V}(\alpha)} Q^\star_{\alpha\beta} = 0$, with $\mathcal{V}\left(\alpha\right)$ the set of connected neighbors. Using Eq 1, this can be written as

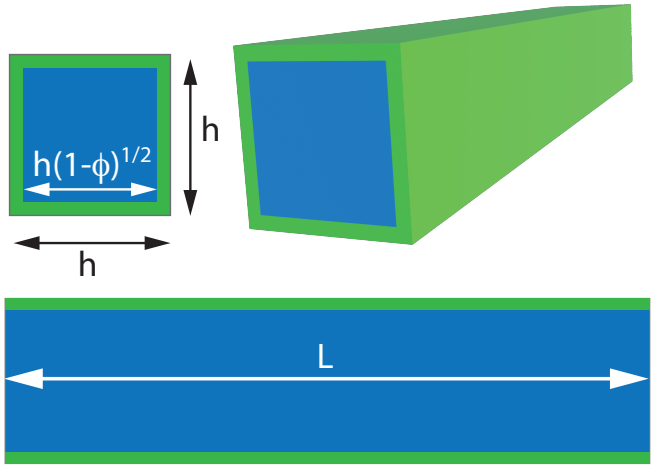
$$\sum_{\beta\in\mathcal{V}(\alpha)} \frac{P^\star_{\alpha\beta}}{R^\star\left(\phi_{\alpha\beta}\right)} = 0. \tag{2}$$

This model is non-dimensionalized as

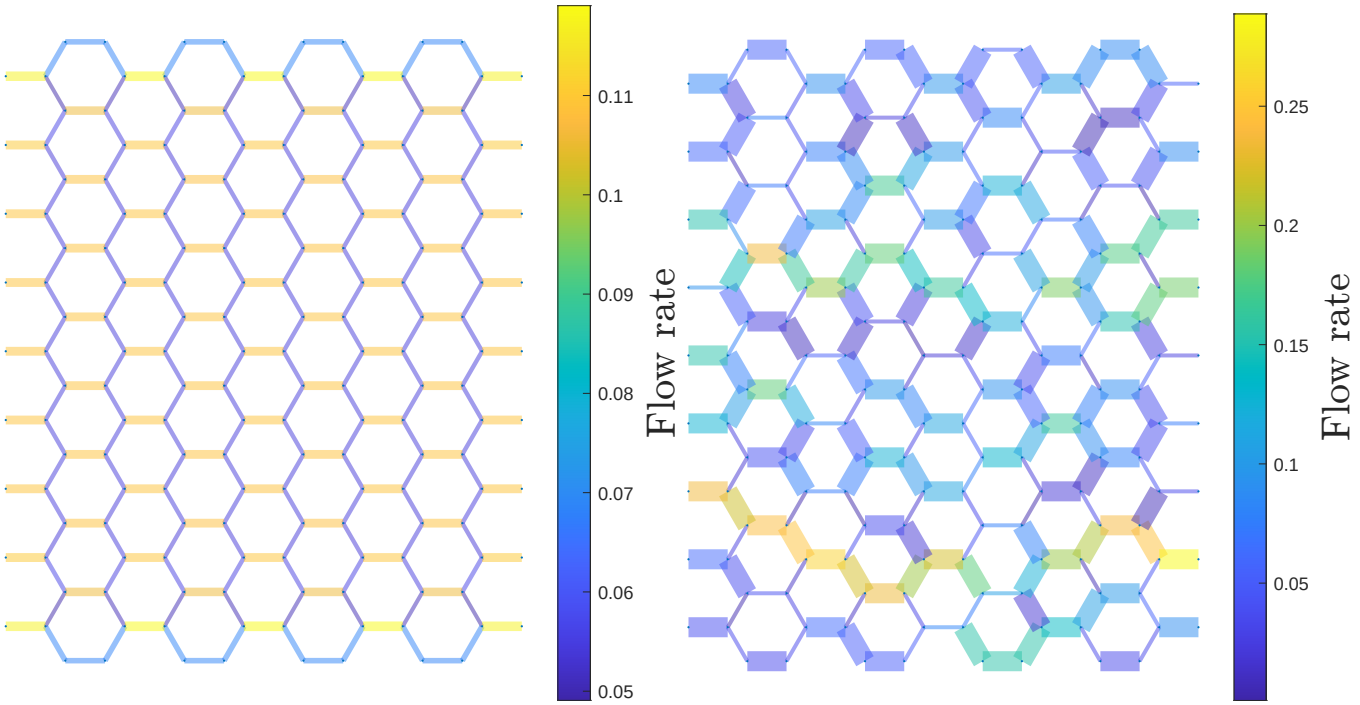
$$\sum_{\beta\in\mathcal{V}(\alpha)} \frac{P_{\alpha\beta}}{R\left(\phi_{\alpha\beta}\right)} = 0, \tag{3}$$

$$R\left(\phi_{\alpha\beta}\right) = \left(1-\phi_{\alpha\beta}\right)^{-2}, \tag{4}$$

with $P_{\alpha\beta} = {}^{P^\star_{\alpha\beta}}/_{(Q_{\text{tot}}R^\star_0)}$, $R\left(\phi_{\alpha\beta}\right) = {}^{R^\star(\phi_{\alpha\beta})}/_{R^\star_0}$ and $Q_{\alpha\beta} = {}^{Q^\star_{\alpha\beta}}/_{Q_{\text{tot}}} = {}^{P_{\alpha\beta}}/_{R(\phi_{\alpha\beta})}$ with $Q_{\text{tot}}$ the total imposed flow rate through the network.




Supplementary figure 1: Geometry of each square cross-section channel in the network with $L = 1$ mm and $h = 100$ µm. Green is the biofilm and blue is the liquid phase. For the analytical solutions and model derivation, we consider a uniform distribution of the biofilm on the surfaces.




(a) Regular hexagonal network

(b) Mixture of channels with width 200 µm and 50 µm

Supplementary figure 2: Simulation of the nondimensional flowrate ($Q_{\alpha\beta}$) distribution in the empty networks with height 100 µm.

*Flow in channels with rectangular cross sections* In the case with rectangular cross sections, all channels share the same height $H = 100$ µm and differ only in their width, which equals 200 µm for the wide channels and 50 µm for the narrow ones. The hydraulic resistance of a rectangular channel depends on its two cross-sectional dimensions, which we label by size: for each channel type $i$ we let $h_i$ denote the smaller dimension and $w_i$ the larger one, so that $w_i > h_i$ by construction. The wide channels then have $h_1 = 100$ and $w_1 = 200$, and the narrow channels have $h_2 = 50$ and $w_2 = 100$, both types satisfying $h_i/w_i = 1/2$. The theoretical expression of the resistance is Bruus [1]

$$\frac{12\mu L}{h_i^3 w_i \left(1 - \sum_{n \text{ odd}} \frac{1}{n^5} \frac{192}{\pi^5} \frac{h_i}{w_i} \tanh\left(n\pi \frac{1}{2h_i/w_i}\right)\right)}.$$

Using $h_i/w_i = 1/2$, we have

$$R_i^\star = B\mu L h_i^{-3} w_i^{-1}, \tag{5}$$

with $B = \frac{12}{1 - \sum_{n \text{ odd}} \frac{1}{n^5} \frac{96}{\pi^5} \tanh(n\pi)}$. Non-dimensionalizing with $R_1^\star$, we obtain

$$\frac{R_2^\star}{R_1^\star} = \left(\frac{h_1}{h_2}\right)^3 \frac{w_1}{w_2} = 16. \tag{6}$$

Non-dimensional flowrate distributions in the empty networks used in the paper are presented in Fig 2.

*Biological development* For each channel, volume fraction evolution is given by

$$\dot{\phi}_{\alpha\beta} = \phi_{\alpha\beta}\left(\underbrace{\Gamma}_{\text{Growth rate}} - \underbrace{g^{\star}_{\alpha\beta}}_{\text{Detachment rate}}\right)(1-\phi_{\alpha\beta}), \tag{7}$$

with $\Gamma$ the growth rate and $g^{\star}_{\alpha\beta}$ the detachment rate. The term $(1-\phi_{\alpha\beta})$ is here to enforce that $\phi_{\alpha\beta} \leq 1$ for $0 < \phi_{\alpha\beta}(t=0) < 1$, the effect of this term can be made steeper close to 1 by using $\left(1-\phi^{n}_{\alpha\beta}\right)$ with $n > 1$ instead of $(1-\phi_{\alpha\beta})$. Initial conditions consist of randomly uniformly distributed values of $\phi_{\alpha\beta}(t=0)$ between 0 and 0.05. For simplicity, in the case of a single genotype, we treat $\Gamma$ $\left[s^{-1}\right]$ as constant throughout the network, with no form of nutrient or oxygen limitation. $g^{\star}_{\alpha\beta}$ $\left[s^{-1}\right]$ describes the detachment rate induced by the average shear stress $\tau^{\star}_{\alpha\beta}$ $[Pa]$ at the biofilm/liquid interface and, similarly to Coyte *et al.* [2], we write this as $g^{\star}_{\alpha\beta} = \chi\sqrt{\tau^{\star}_{\alpha\beta}}$ with $\chi$ $\left[Pa^{-\frac{1}{2}} \times s^{-1}\right]$ the erosion rate.

The average shear stress $\tau^{\star}_{\alpha\beta}$ can be readily derived either from the expression of the velocity field on the surface or by considering that the shear force on the liquid/biofilm is equal to the force of the pressure differential between inlet and outlet of the fluid flow. To use the second method, consider that the surface of the square cross-section in which fluid flows is $h^2(1-\phi_{\alpha\beta})$ and that the surface of the liquid/biofilm interface is $4h(1-\phi_{\alpha\beta})^{\frac{1}{2}}$ (Fig 1). We therefore have $P^{\star}_{\alpha\beta}h^2(1-\phi_{\alpha\beta}) = \tau^{\star}_{\alpha\beta}4h(1-\phi_{\alpha\beta})^{\frac{1}{2}}L$ in the square cross-section channels, so that $\tau^{\star}_{\alpha\beta} = {}^{P^{\star}_{\alpha\beta}h(1-\phi_{\alpha\beta})^{\frac{1}{2}}}\!/_{(4L)}$. Using Darcy's law for each channel, $P^{\star}_{\alpha\beta} = R^{\star}_{0}(1-\phi_{\alpha\beta})^{-2}Q^{\star}_{\alpha\beta}$ with $R^{\star}_{0} = A\mu L h^{-4}$, this can be expressed as $\tau^{\star}_{\alpha\beta} = {}^{A}\!/_{4}\mu h^{-3}(1-\phi_{\alpha\beta})^{-\frac{3}{2}}Q^{\star}_{\alpha\beta}$.

In our model, we further capture sloughing events by considering that there is a critical value of the total stress at the biofilm/solid interface, $\sigma^{\star}_{\text{crit}}$ $[Pa]$, that induces a near complete detachment of the biofilm

$$\phi_{\alpha\beta} = \phi_{\alpha\beta}(t=0) \text{ if } \sigma^{\star}_{\alpha\beta} \geq \sigma^{\star}_{c}. \tag{8}$$

The total stress at the biofilm/solid interface is calculated as the sum of the effect of the shear and pressure forces on the biofilm and translated into a stress at the biofilm/solid interface. This leads to $\sigma^{\star}_{\alpha\beta} = \frac{h^2 P^{\star}_{\alpha\beta}}{4hL}$, which can be written as $\sigma^{\star}_{\alpha\beta} = {}^{A}\!/_{4}\mu h^{-3}(1-\phi_{\alpha\beta})^{-2}Q^{\star}_{\alpha\beta}$.

This model is non-dimensionalized, for any channel $\alpha\beta$, as

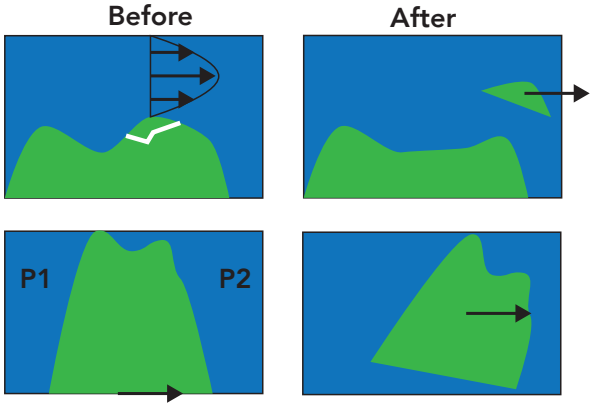
$$\begin{cases} \dot{\phi}_{\alpha\beta} & = \phi_{\alpha\beta}(1-g_{\alpha\beta})(1-\phi_{\alpha\beta}), \text{if } \phi_{\alpha\beta} < 1-\sqrt{\Lambda_c Q_{\alpha\beta}} \\ \phi_{\alpha\beta}(\tau=0) & \text{if } \phi_{\alpha\beta} \geq 1-\sqrt{\Lambda_c Q_{\alpha\beta}} \end{cases} \tag{9}$$

with dimensionless time $\tau = t\Gamma$. The dimensionless parameter $\Lambda_c$, which characterizes the sensitivity to sloughing detachment, reads $\Lambda_c = \frac{A\mu}{4h^3}\frac{Q_{\text{tot}}}{\sigma_c}$. It can also be expressed as $\Lambda_c = \frac{Q_{\text{tot}}}{Q_c}$ with $Q_c = \sigma_c\frac{4h^3}{A\mu}$ or as $\Lambda_c = \frac{\sigma_{ref}}{\sigma_c}$ with $\sigma_{ref} = \frac{A\mu}{4h^3}Q_{\text{tot}}$. We further have

$$g_{\alpha\beta} = \sqrt{\frac{\chi^2}{\Gamma^2}\tau^{\star}_{\alpha\beta}} = \sqrt{\Lambda_s Q_{\alpha\beta}}(1-\phi_{\alpha\beta})^{-\frac{3}{4}}. \tag{10}$$

The dimensionless parameter $\Lambda_s$, which characterizes the sensitivity to shear detachment, reads $\Lambda_s = \frac{A\mu\chi^2}{4h^3\Gamma^2}Q_{\text{tot}}$. It can also be expressed as $\Lambda_s = {}^{Q_{\text{tot}}}\!/_{Q_s}$ with $Q_s = \frac{4h^3\Gamma^2}{A\mu\chi^2}$ or $\Lambda_s = {}^{\tau_0}\!/_{\tau_s}$ with $\tau_0 = \frac{A\mu}{4h^3}Q_{\text{tot}}$ and $\tau_s = \frac{\Gamma^2}{\chi^2}$. In the case of a single microchannel with imposed flow rate, equilibrium between growth and detachment is reached for $\sqrt{\Lambda_s}(1-\phi_{\text{equ}})^{-\frac{3}{4}} = 1$ so $\phi_{\text{equ}} = 1-\Lambda_s^{2/3}$. Cycles of sloughing and re-growth occur if $1-\Lambda_c^{1/2} \leq 1-\Lambda_s^{2/3}$ so if $\Lambda_c \geq \Lambda_s^{4/3}$.

**Summary of detachment modes and corresponding dimensionless numbers:**




**Mode of detachment 1:**
shear-induced, detachment from biofilm due to stress at the biofilm/flow interface

**Sensitivity to mode 1:**
dimensionless number

$\Lambda_S$

**Mode of detachment 2:**
pressure-induced, detachment from substrate due to stress at the biofilm/substrate interface

**Sensitivity to mode 2:**
dimensionless number

$\Lambda_C$

[1] H. Bruus, *Theoretical Microfluidics* (Oxford University Press, 2007).
[2] K. Z. Coyte, H. Tabuteau, E. A. Gaffney, K. R. Foster, and W. M. Durham, Proceedings of the National Academy of Sciences **114**, E161 (2017).

## II. COMPETITION MODEL IN THE NETWORK

We use a similar approach to model exploitative bacterial competition in the network, but taking into account a form of nutrient limitation and also the difference in growth rates between the two bacteria, $A$ and $B$. The flow equations are identical to that presented in the previous section. For volume fraction development, we have the non-dimensional equations

$$\begin{cases} \dot{\phi}^A_{\alpha\beta} & = \phi^A_{\alpha\beta}\left(\gamma_{\alpha\beta} - g^A_{\alpha\beta}\right)\left(1-\phi^A_{\alpha\beta}\right), \text{if } \phi^A_{\alpha\beta} < 1 - \sqrt{\Lambda^A_c Q_{\alpha\beta}} \\ \phi^A\left(\tau = 0\right) & \text{if } \phi^A_{\alpha\beta} \geq 1 - \sqrt{\Lambda^A_c Q_{\alpha\beta}} \end{cases}, \tag{11}$$

and

$$\begin{cases} \frac{\Gamma^A}{\Gamma^B}\dot{\phi}^B_{\alpha\beta} & = \phi^B_{\alpha\beta}\left(\gamma_{\alpha\beta} - g^B_{\alpha\beta}\right)\left(1-\phi^B_{\alpha\beta}\right), \text{if } \phi^B_{\alpha\beta} < 1 - \sqrt{\Lambda^B_c Q_{\alpha\beta}} \\ \phi^B\left(\tau = 0\right) & \text{if } \phi^B_{\alpha\beta} \geq 1 - \sqrt{\Lambda^B_c Q_{\alpha\beta}} \end{cases}, \tag{12}$$

with dimensionless time $\tau = t\Gamma^A$ and similar notations as before. In each channel only one of the two strains is present: half of the channels are randomly assigned to A and the other half to B, so that the two strains never share a channel and their volume fractions are mutually exclusive. Each channel therefore follows the single-strain dynamics of the previous section. The dimensionless numbers are therefore $\Lambda^A_c,\ \Lambda^A_s$ for $A$, $\Lambda^B_c,\ \Lambda^B_s$ for $B$ and the ratio of growth rates $\frac{\Gamma^A}{\Gamma^B}$. To take into account nutrient limitation due the competition between transport and reaction, we consider that

$$\begin{cases} \gamma_{\alpha\beta} & = 1, \text{if } Q_{\alpha\beta} > 10^{-6} \\ \gamma_{\alpha\beta} & = 10^{-3}, \text{if } Q_{\alpha\beta} \leq 10^{-6} \end{cases}. \tag{13}$$

The idea of this approach is simply to reduce the growth rate by several orders of magnitude when the channel is completely clogged and advection cannot transport nutrients to the biofilm. For each bacteria, the fitness metric for each channel is $\gamma_{\alpha\beta}$ and the global fitness is the average value of $\gamma_{\alpha\beta}$ over the colonized channels.

## III. SUPPLEMENTARY EXPERIMENTAL RESULTS

### A. *Pseudomonas aeruginosa* in regular networks

#### 1. Supplementary Videos

*Supplementary Video 1:* Biofilm colonization in the ordered network. *Pseudomonas aeruginosa*. One week at 2 µl/min. Time step 1 h. Bright-field.

*Supplementary Video* 2: Biofilm colonization in the ordered network. *Pseudomonas aeruginosa*. One week at 2 µl/min. Time step 1 h. GFP.

*Supplementary Video 3:* Biofilm colonization in the ordered network. *Pseudomonas aeruginosa*. 70 h at 20 µl/min. Time step 1 h. Bright-field.

*Supplementary Video 4:* Biofilm colonization in the ordered network. *Pseudomonas aeruginosa*. 70 h at 20 µl/min. Time step 1 h. GFP.

*Supplementary Video 5:* Biofilm colonization in the ordered network. *Pseudomonas aeruginosa*. 70 h at 200 µl/min. Time step 1 h. Bright-field.

*Supplementary Video 6:* Biofilm colonization in the ordered network. *Pseudomonas aeruginosa*. 70 h at 200 µl/min. Time step 1 h. GFP.

#### 2. Definition of $\langle\delta(t)\rangle_{x,y}$,$\langle\delta(x,y)\rangle_t$ and $\langle I(t)\rangle_{x,y}$

We define $\langle\delta(t)\rangle_{x,y}$, the spatially-averaged RMS of $\partial_t I$ as

$$\langle\delta(t)\rangle_{x,y} = \sqrt{\frac{1}{M}\sum_{x,y}\partial_t I(x,y,t)^2},$$

where $M$ is the total amount of pixels within the image $I$, $x$ and $y$ are the pixel coordinates, $t$ is the time, and the time derivative of the image sequence $\partial_t I$ is computed as $\frac{I_{t+1}-I_t}{\Delta t}$ with $\Delta t = 1$h. To separate the analysis between biofilm growth and detachment, we split the time derivative into a positive ($\partial_t I^+$ growth) and negative ($\partial_t I^-$ detachment) values

$$\partial_t I^+ = \partial_t I \geq 0$$
$$\partial_t I^- = \partial_t I \leq 0$$

Using these values, we compute the spatially-averaged RMS of $\partial_t I^+$ and $\partial_t I^-$

$$\langle\delta^+(t)\rangle_{x,y} = \sqrt{\tfrac{1}{M}\textstyle\sum_{x,y}\partial_t I^+(x,y,t)^2},\ \ \langle\delta^-(t)\rangle_{x,y} = \sqrt{\tfrac{1}{M}\textstyle\sum_{x,y}\partial_t I^-(x,y,t)^2}.$$

Following the same idea, we define $\langle\delta(x,y)\rangle_t$, the time-averaged RMS of $\partial_t I$, considering independently the growth and detachment as well

$$\langle\delta(x,y)\rangle_t = \sqrt{\tfrac{1}{N}\textstyle\sum_t\partial_t I(x,y,t)^2},\ \ \langle\delta^+(x,y)\rangle_t = \sqrt{\tfrac{1}{N}\textstyle\sum_t\partial_t I^+(x,y,t)^2},\ \ \langle\delta^-(x,y)\rangle_t = \sqrt{\tfrac{1}{N}\textstyle\sum_t\partial_t I^-(x,y,t)^2}$$

where $N$ is the total amount of pictures in the image sequence.

Finally, we define the average pixel intensity, that accounts for biomass, as

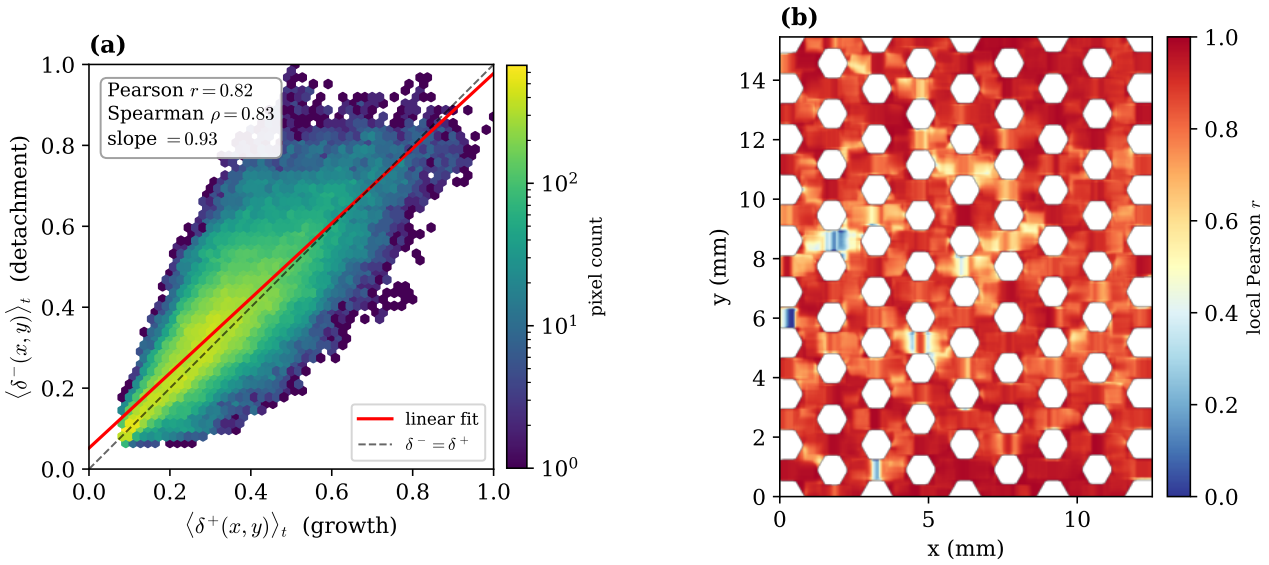
$$\langle I(t)\rangle_{x,y} = \frac{1}{M}\sum_{x,y} I(x,y,t)$$

and then the signal is normalized using its maximum value.

### 3. *Correlation between growth and detachment maps*

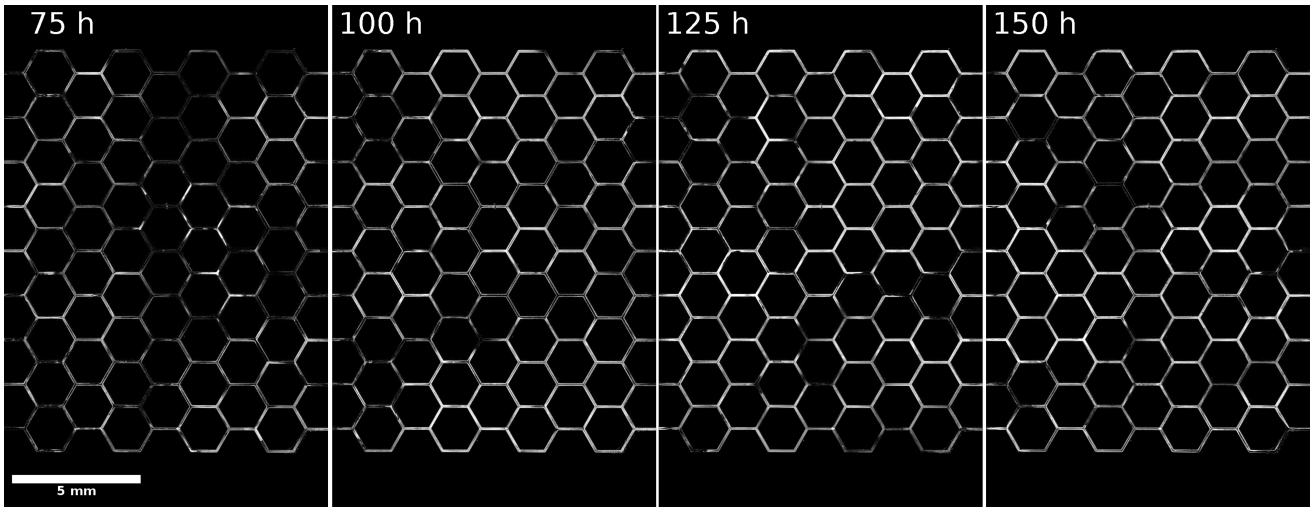
To quantify the visual correlation between the spatial patterns of growth and detachment observed in Fig 1c of the manuscript, we compared the two time-averaged maps $\langle \delta^+(x,y) \rangle_t$ (growth) and $\langle \delta^-(x,y) \rangle_t$ (detachment) pixel by pixel, restricting the analysis to the pixels belonging to the channel network (where both quantities are defined). The joint distribution of the two maps is shown in Supplementary figure 3a. The two quantities are strongly and positively correlated, with a Pearson correlation coefficient $r \approx 0.82$ and a Spearman rank correlation coefficient $\rho \approx 0.83$. A linear fit gives a slope close to unity ($\approx 0.93$), indicating that the local magnitudes of growth and detachment are not only correlated but of comparable amplitude.

This correlation is not an artifact of both maps sharing the same channel skeleton. First, it is essentially unchanged when the maps are coarse-grained: averaging both quantities within square regions of increasing size, from a few pixels up to the scale of an individual channel ($\sim 1.3$ mm), leaves the coefficient in the range $r \approx 0.80$ to 0.83. Second, a local Pearson coefficient computed within sliding windows (of size $\sim 0.65$ mm) is high and spatially uniform across the whole network (median $r \approx 0.89$, Supplementary figure 3b), showing that growth and detachment are co-located everywhere rather than only in specific sub-regions. Finally, to verify that the correlation reflects the pairing of intensity values rather than the mere fact that both maps are defined on the same channel skeleton, we performed a label-permutation test: keeping the same set of channel pixels but randomly shuffling the detachment values among them destroys the correlation completely ($r \approx 0.00 \pm 0.004$ over 1000 permutations, two-sided $p < 10^{-3}$), whereas the observed value is $r \approx 0.82$. Because this test leaves the network geometry and the distribution of intensity values unchanged and only removes the spatial pairing between the two maps, the collapse of the coefficient can only be attributed to the intensities being correlated in space. A rigid spatial shift of the detachment map relative to the growth map by a few channel widths also lowers the coefficient (to $r \approx 0.18$), although in that case part of the decrease is geometric, since the shifted network no longer overlaps itself; the permutation test is thus the cleaner control. These controls confirm that the correlation arises from the spatial co-location of the growth and detachment intensities and not from the shared network geometry. Taken together, these analyses provide a quantitative confirmation that regions of enhanced biomass growth also experience enhanced detachment.



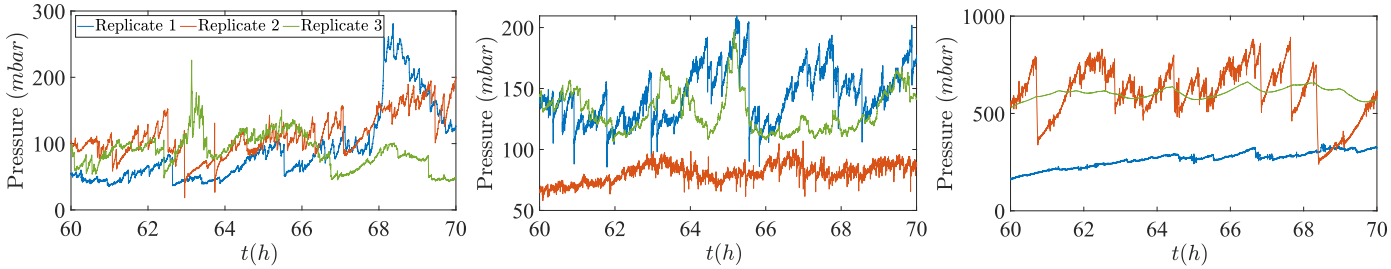

Supplementary figure 3: Quantification of the spatial correlation between the growth map $\langle \delta^+(x,y) \rangle_t$ and the detachment map $\langle \delta^-(x,y) \rangle_t$ of Fig 1c. (a) Pixel-wise joint distribution of the two maps (logarithmic colour scale) with the linear fit (red) and the identity line $\delta^- = \delta^+$ (dashed). The Pearson coefficient is $r \approx 0.82$, the Spearman coefficient $\rho \approx 0.83$ and the fitted slope $\approx 0.93$. (b) Map of the local Pearson coefficient computed within sliding windows ($\sim 0.65$ mm), which remains high and spatially uniform across the network.

## 4. Supplementary figures



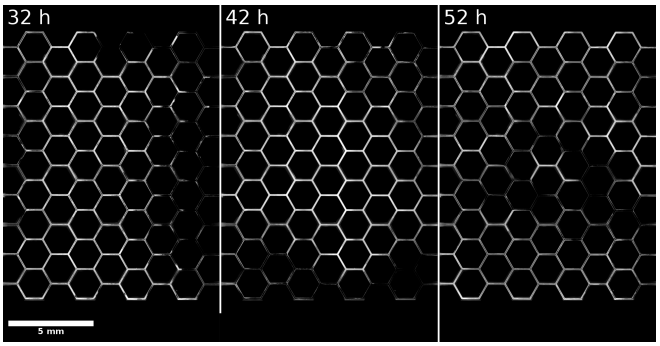

(a)

Supplementary figure 4: Bright-field images showing the colonization of biofilm inside the network. These images correspond to Fig 1 in the manuscript. Scale bar 5 mm.

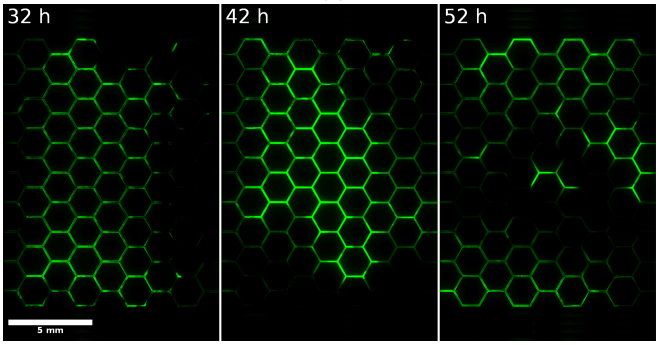



(a) (b) (c)

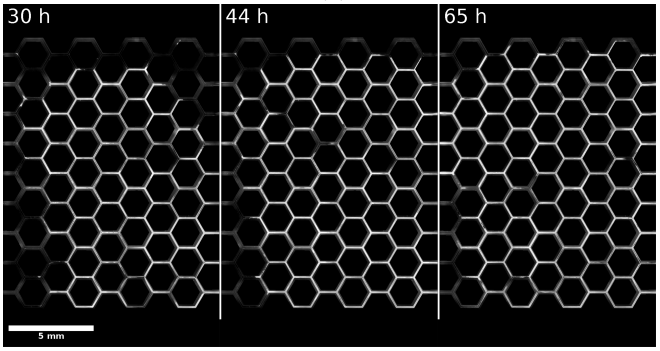
Supplementary figure 5: Pressure for three different replicates at three flow rates. (a) 2 µl/min, (b) 20 µl/min (c) 200 µl/min. The third experiment, in green, for the case 200 µl/min was performed using a Fluigent XL flow-meter and the other two replicates using an L flow-meter, hence the difference in sensor response.



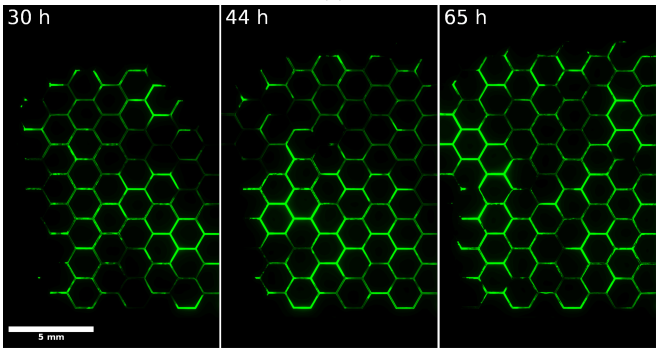

(a)




(b)

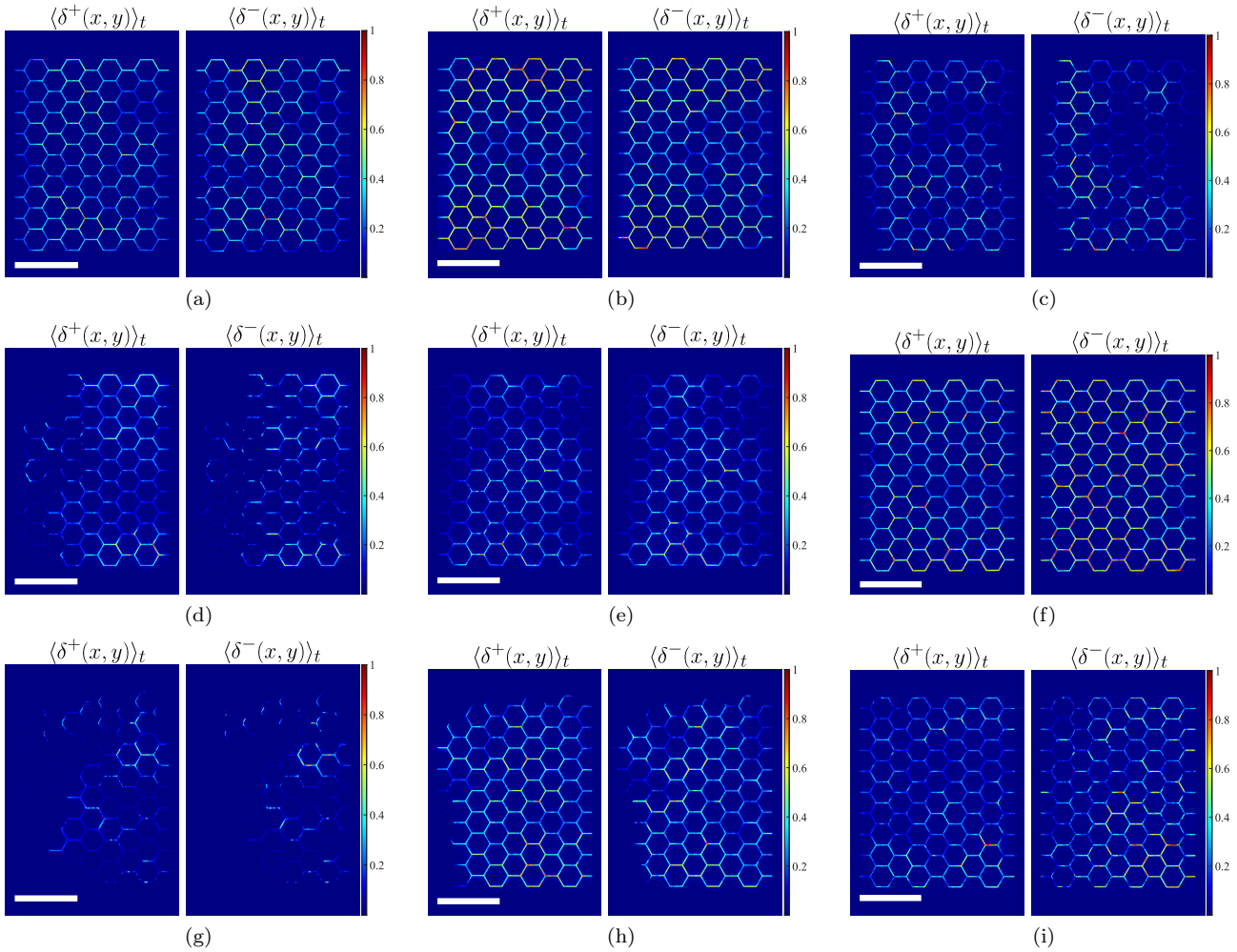



(c)

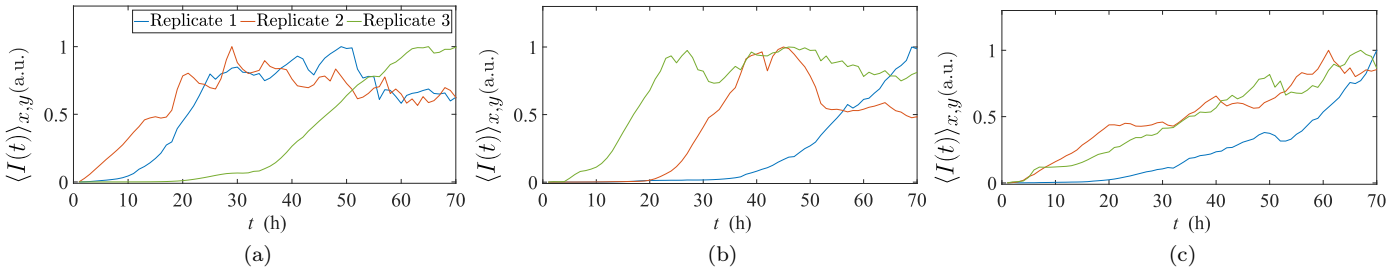



(d)

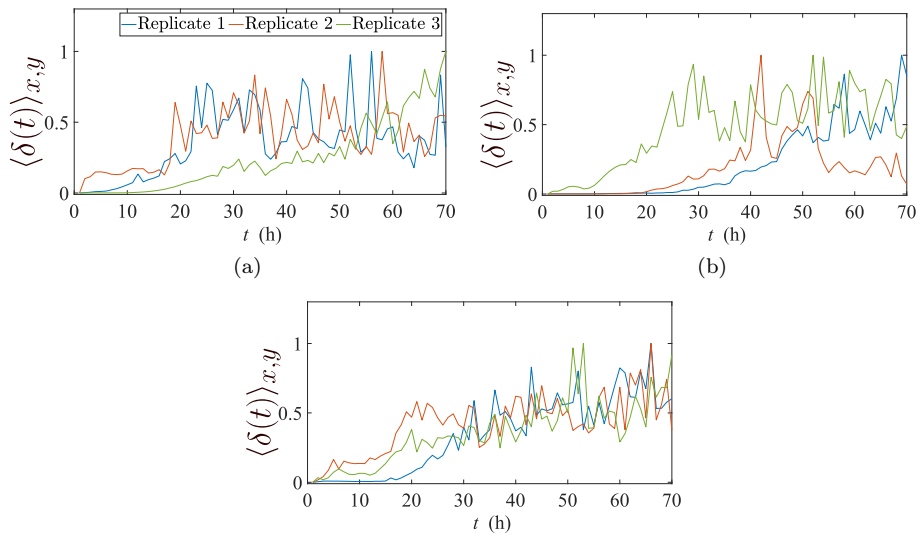
Supplementary figure 6: Example of biofilm colonization at different flow rates. (a) Bright-field and (b) GFP images at three different moments at 20 µl/min. (c) Bright-field and (d) GFP images at three different moments at 200 µl/min. Scale bar 5 mm.



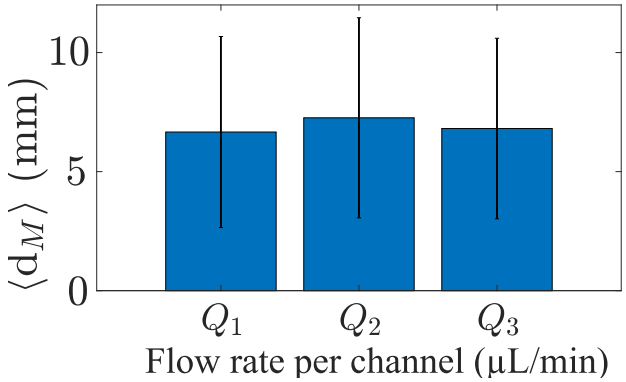

Supplementary figure 7: Time integrated RMS of the GFP intensity for all replicates at different flow rates during 70 h. (a), (b) and (c) 2 µl/min. (d), (e) and (f) 20 µl/min. (g), (h) and (i) 200 µl/min. Scale bar 5 mm.




Supplementary figure 8: Integrated GFP intensity for all replicates at different flow rates. (a) 2 µl/min (b) 20 µl/min and (c) 200 µl/min.

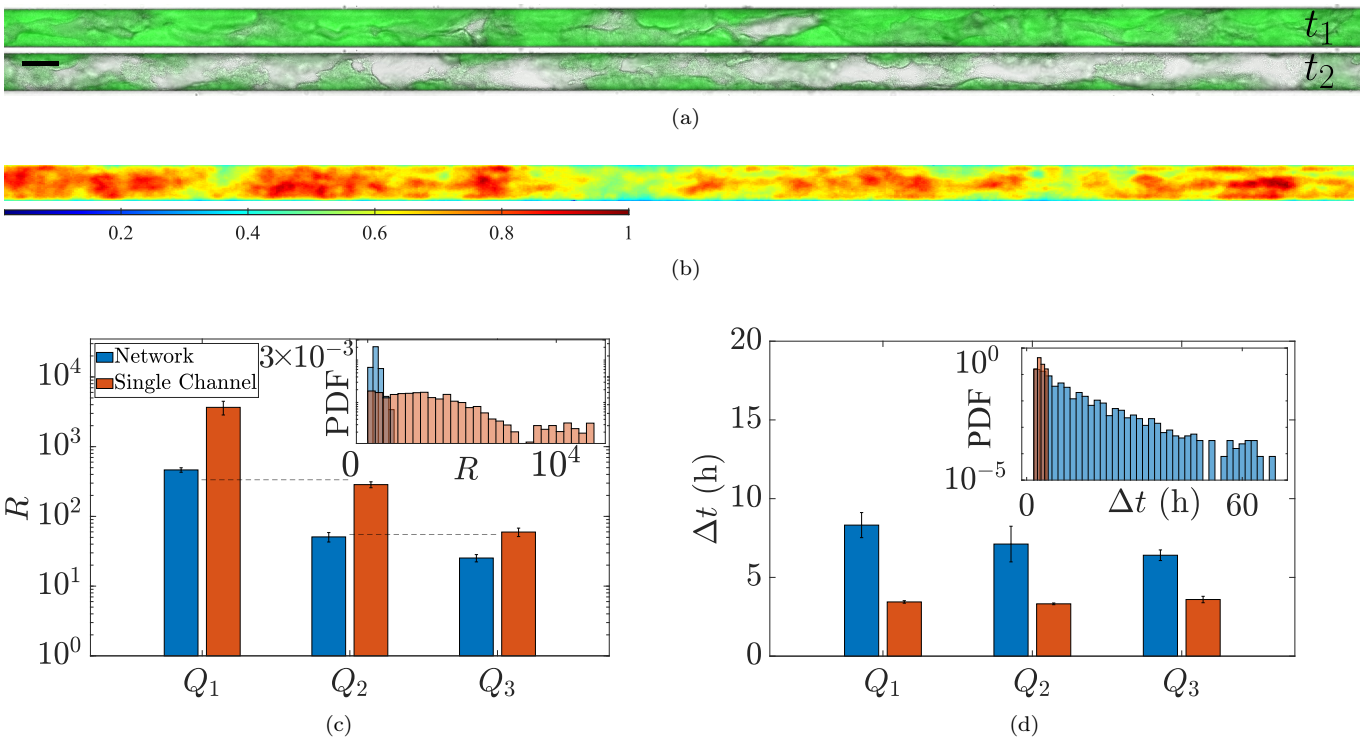



Supplementary figure 9: Space integrated RMS of GFP intensity for all replicates at different flow rates. (a) 2 µl/min (b) 20 µl/min and (c) 200 µl/min.




Supplementary figure 10: Mean values of $d_M$ at different flow rates. The mean value was obtained by averaging all data of three replicates for each flow rate shown in the distribution of $d_M$. Error bars are the standard deviation. Flow rates $Q_1$, $Q_2$ and $Q_3$ correspond to 2, 20 and 200 µl/min.

### B. *Pseudomonas aeruginosa* in single channels




Supplementary figure 11: Comparison between network and single channel experiments. (a) Composite image of bright field and fluorescence showing a sloughing event in a single channel. Biofilm clogs the channel ($t_1$, top), leading to an increase in hydraulic resistance, shear stress and pressure and ultimately to biomass detachment ($t_2$, bottom). (b) Time-averaged RMS of $\partial_t I$, $\langle \delta(x,y) \rangle_t$, showing fluctuations of biofilm growth and detachment within a single channel. (c) Normalized hydraulic resistance at three flow rates $Q_1$, $Q_2$ and $Q_3$ for the complete network and a single channel. Inset: Example distribution of hydraulic resistance for the case $Q_1$ showing all the values found within three replicates. (d) Time between detachments $\Delta t$. Every detachment corresponds to peaks in the intensity signal. The statistics are calculated for each channel individually within the network and compared with the single channel experiment. Inset: Example distribution of $\Delta t$ for the case $Q_1$ showing all the values found within three replicates. The flow rate in (a) and (b) is 2 µl/min and the scale bar is 100 µm. The values in (c) and (d) are the means with error bars corresponding to the standard error . The mean value for each condition was computed by averaging the mean value of every experiment, using three replicates. The flow rates $Q_1$, $Q_2$ and $Q_3$ correspond to 2, 20 and 200 µl/min for the network and 0.2, 2 and 20 µl/min for single channel experiments, so as to correspond to approximately the same velocity in the empty network.

### C. *Staphylococcus aureus* in regular networks

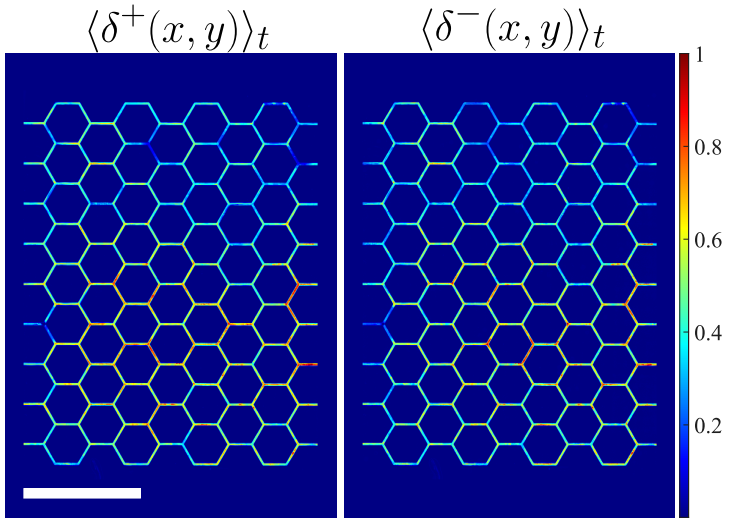
#### 1. Supplementary Videos

*Supplementary Video 7:* Biofilm colonization in the ordered network. *Staphylococcus aureus*. 120 h at 2 µl/min. Time step 0.5 h. Bright-field.

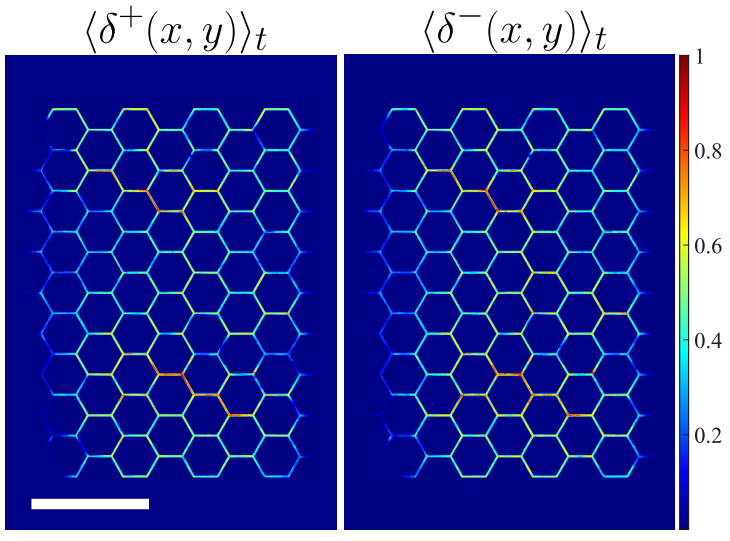
*Supplementary Video 8:* Biofilm colonization in the ordered network with fibronectin coating. *Staphylococcus aureus*. 120 h at 2 µl/min. Time step 0.5 h. Bright-field.

#### 2. Supplementary figures

Experiments in networks using *Staphylococcus aureus* were recorded and analyzed in bright-field.

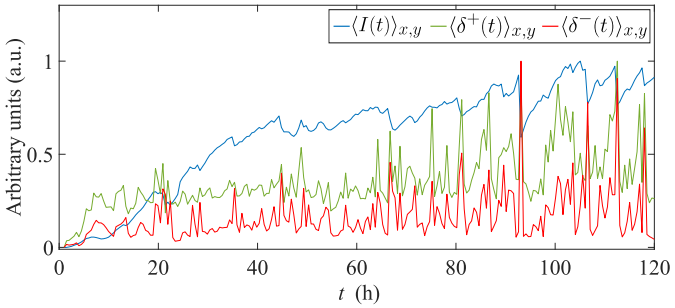



(a)

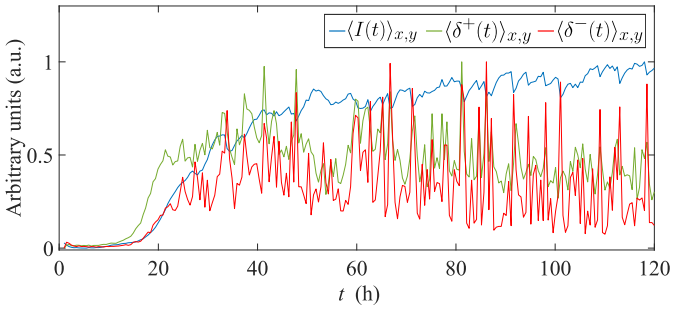



(b)

Supplementary figure 12: Time integrated RMS of the bright-field intensity for two conditions. (a) Main experiment and (b) fibronectin-coated chip.

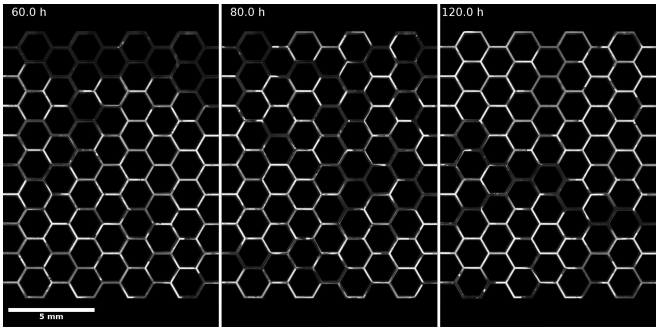



(a)

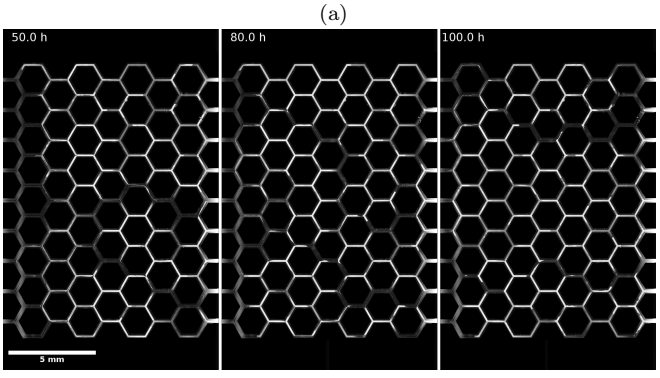



(b)

Supplementary figure 13: Space integrated RMS bright-field intensity for two conditions. (a) Main experiment and (b) fibronectin-coated chip.




(a)




(b)

Supplementary figure 14: Example of biofilm colonization in bright-field for two conditions (a) Main experiment and (b) fibronectin-coated chip. Scale bar 5 mm.

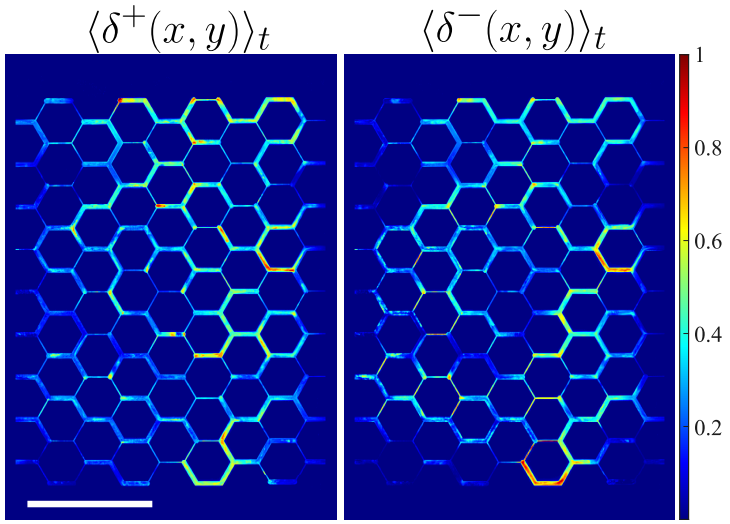
## D. *Pseudomonas aeruginosa* in disordered networks

### 1. Supplementary Videos

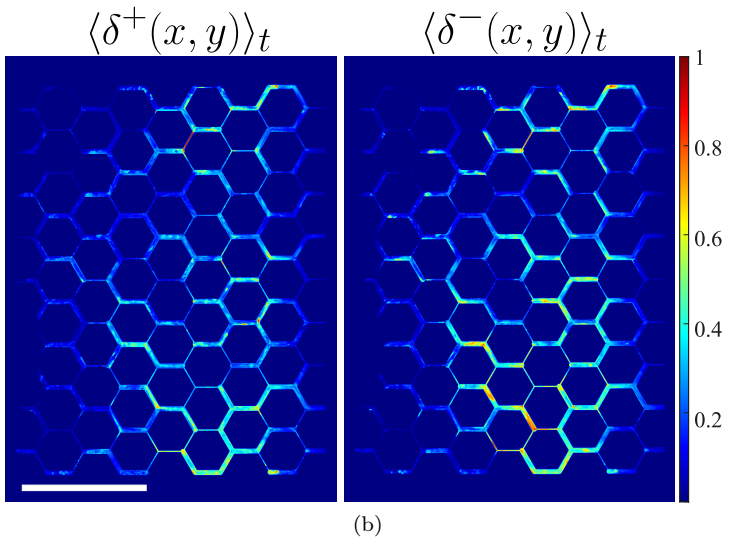
*Supplementary Video 9:* Biofilm colonization in the disordered network. *Pseudomonas aeruginosa*. 70 h at 2 µl/min. Time step 1 h. Bright-field.

*Supplementary Video 10:* Biofilm colonization in the disordered network. *Pseudomonas aeruginosa*. 70 h at 2 µl/min. Time step 1 h. GFP.

### 2. Supplementary figures

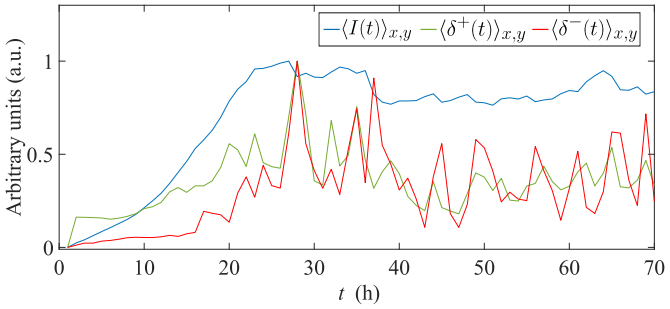



(a)

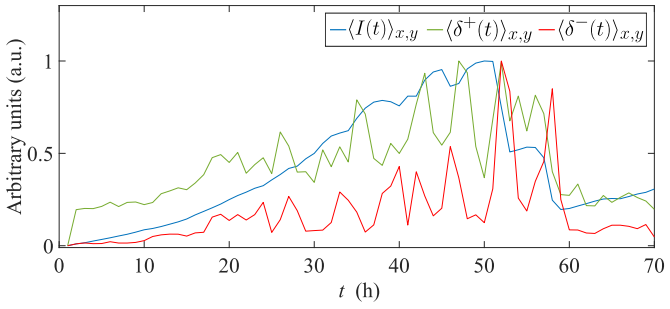



(b)

Supplementary figure 15: Triplicate: time-integrated RMS of the GFP intensity for the two replicates shown here, in addition to the one in the main text, at 2 µl/min during 70 h. The network has two channel width, 50 µm and 200 µm, positioned randomly. (a) Replicate 1 (b) Replicate 2. Scale bar 5 mm.

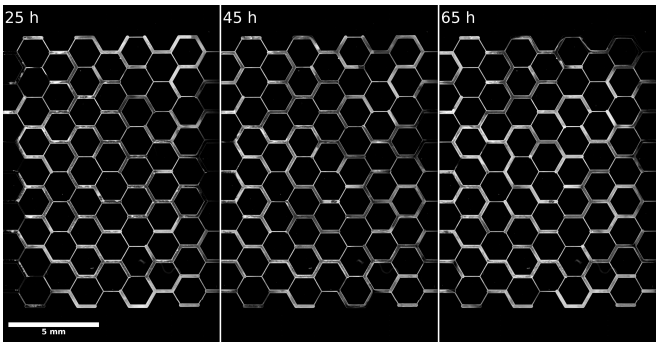



(a)

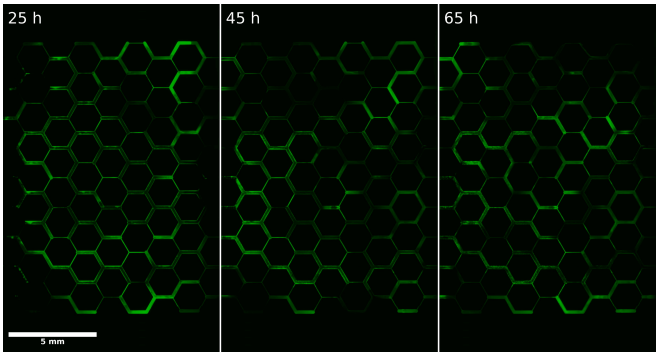



(b)

Supplementary figure 16: Triplicate: space-integrated RMS of the GFP intensity for the two replicates shown here, in addition to the one in the main text, at 2 µl/min during 70 h. (a) Replicate 1 (b) Replicate 2. Scale bar 5 mm.




(a)




(b)

Supplementary figure 17: Example of biofilm colonization at 2 µl/min within the network with two channel width (Replicate 1). (a) Bright-field images (b) GFP images. Scale bar 5 mm.

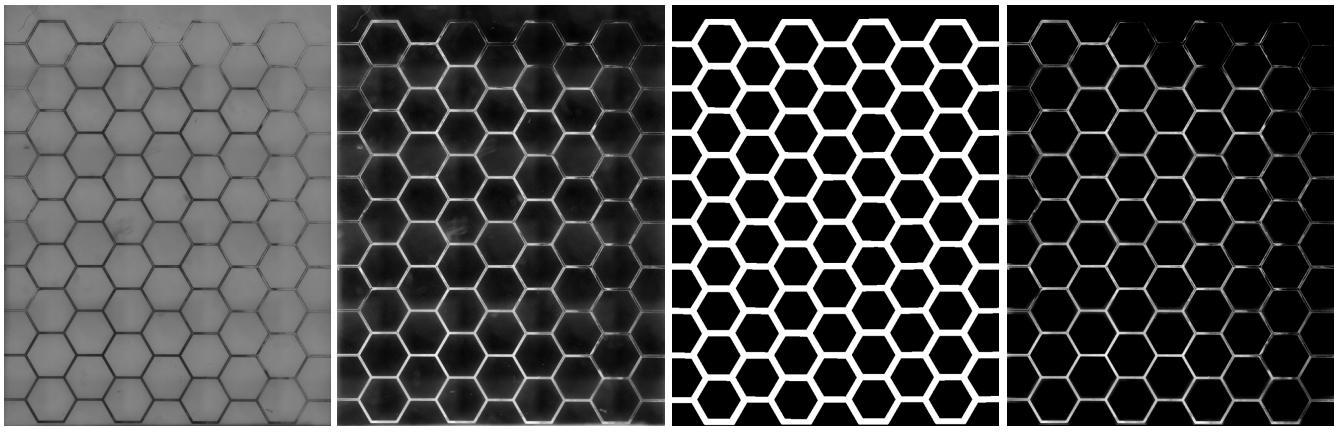
Contrary to the regular network, in which the flow in the empty geometry is nearly homogeneous, the disordered network exhibits a heterogeneous flow distribution even before biofilm growth. This is a direct consequence of the channel-width disorder: the wider channels have a much smaller hydraulic resistance (by a factor of about 16 for the two widths used here, see Eq. 6) and thus carry most of the flow, forming preferential flow paths already in the empty network (Supplementary figure 2b). As biofilm develops, growth and detachment are enhanced along these pre-existing high-flow channels, which explains the localized regions of elevated RMS of the intensity signal observed in Supplementary figures 15a and 15b.

### E. *Pseudomonas aeruginosa* in single channels

*Supplementary Video 11:* Biofilm colonization in a single channel. *Pseudomonas aeruginosa*. 73.5 h at 2 μl/min. Time step 0.5 h. GFP.

## IV. IMAGE TREATMENT FOR BRIGHT-FIELD IMAGES

Images in bright-field were treated to improve visualization of biofilm inside the network and remove imaging noise outside the channel network. The treatment consists in inverting the colors of the image and then applying a mask. The resulting image shows biofilm as bright structures within the network.

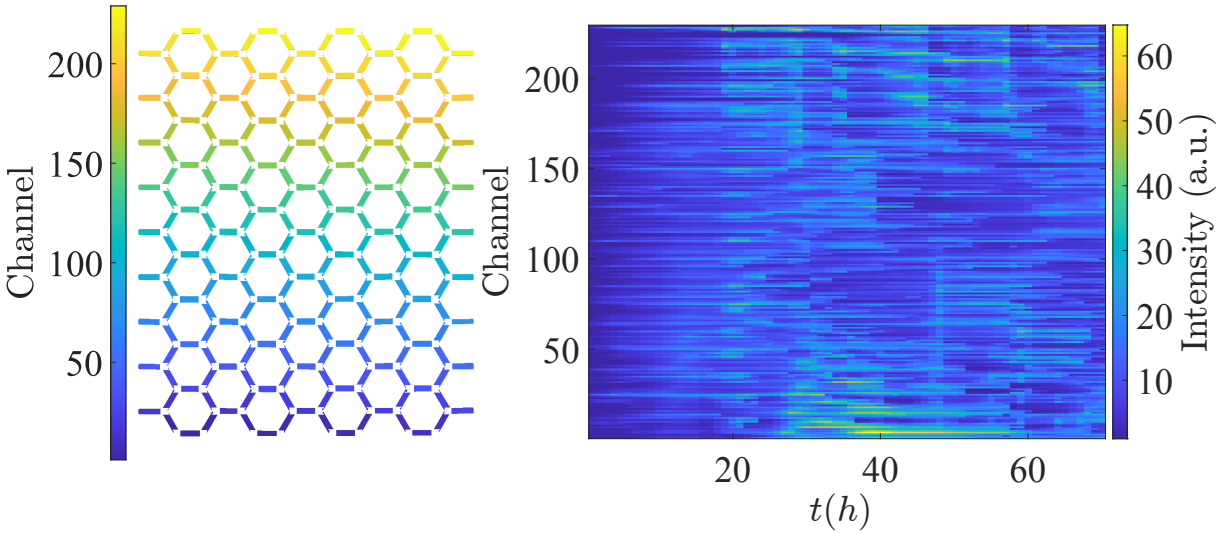


(a) (b) (c) (d)

Supplementary figure 18: Example of image treatment in bright-field. (a) Raw image (b) Inverted image. (c) Mask. Black are zeros and white are ones. (d) Final image.

## V. IMAGE TREATMENT FOR OBTAINING $\Delta t$ AND $d_M$ IN FIGURES 1 AND 3

GFP image sequences were treated using a mask to label each channel inside the network. Using the mask, the intensity of each channel is integrated in space and labeled from 1 to 229 and the coordinates of each labeled channel within the network are known. This treatment allows us to detect the moment and position of detachment events, corresponding to peaks (local maxima) in the intensity signal $\langle I(t)\rangle_{ch}$. For detecting the peaks, we use a custom script in Matlab to proceed as follows. First, we obtain the time derivative from the normalized intensity signal $\langle I(t)\rangle_{ch}$as $\partial_t\langle I(t)\rangle_{ch} = \frac{\langle I(t+1)\rangle_{ch} - \langle I(t)\rangle_{ch}}{\Delta t}$, with $\Delta t = 1$h. As we are interested in detachments, we only keep the negative values of the derivative ($\partial_t\langle I(t)\rangle^-_{ch} = \partial_t\langle I(t)\rangle_{ch} < 0$). Then, for simplicity, we analyze the absolute value $|\partial_t\langle I(t)\rangle^-_{ch}|$, and we normalize it with the intensity signal $\langle I(t)\rangle_{ch}$ in order to have the percentage of biomass loss $\frac{|\partial_t\langle I(t)\rangle^-_{ch}|}{\langle I(t)\rangle_{ch}}$. To avoid considering noise (false detachments) from the beginning of the experiment, we analyze the values of $\frac{|\partial_t\langle I(t)\rangle^-_{ch}|}{\langle I(t)\rangle_{ch}}$ in which $\langle I(t)\rangle_{ch} > 0.1$ (enough observed biofilm). The resulting signal has several zeros, and non-zero values corresponding to the biomass loss percentage. In a group of biomass loss, we consider the first value as a detachment event, and the rest of values as a continuation of the same event. With this definition, the detachment events correspond to the peaks in the intensity signal $\langle I(t)\rangle_{ch}$, as shown in Figure 1d of the manuscript. We analyze the signal of every channel in the network, and we save the time $t$ and position $x, y$ of every detachment. Figure 19 shows a map of the intensity per channel in time $\langle I(t)\rangle_{ch}$. Within a single channel, $\Delta t$ is defined as the time between two consecutive peaks, or time between detachments. We obtained the distribution of $\Delta t$ for all channels in the network in three replicates for each flow rate. At any given time $t$, detachments can occur in different channels. We identified the maximum detachment in the network as the maximum peak within all channels at time $t$, and then, we calculated the distance between two consecutive maximum detachments $d_M$ as $\sqrt{(x_m(t+1) - x_m(t))^2 + (y_m(t+1) - y_m(t))^2}$, where $x_m(t)$ and $y_m(t)$ are the coordinates of the channel with maximum detachment at a time $t$.

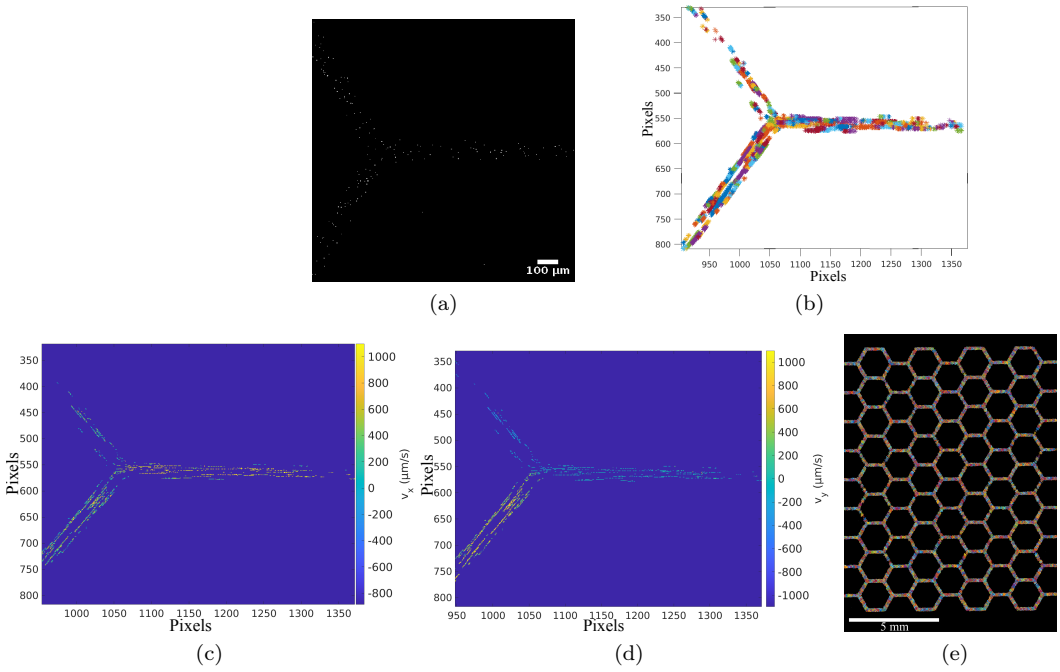



(a) (b)

Supplementary figure 19: (a) Mask containing labeled channels from 1 to 229. The mask only takes the inner part of each channel, to avoid overlapping of data in the intersections. (b) Map containing the resulting intensity per channel at different times. Notice that each decrease in intensity correspond to detachments.

## VI. PARTICLE TRACKING VELOCIMETRY (PTV)

### A. PTV analysis steps




Supplementary figure 20: Summary of the different steps used for particle tracking velocimetry. (a) Example of channels containing beads in one of the mosaic section to reconstruct the complete network. The grayscale image corresponds to the red fluorescence of the particles. Each bead is detected individually and then the trajectories are assigned. (b) Example of the trajectories detected after tracking. Each color represents a different trajectory. (c) and (d) Maps containing the resulting values for the velocity component $v_x$ and $v_y$, respectively and for each detected trajectory. A mask containing labels for each channel is then applied and all the values within a channel are averaged before obtaining $v_\alpha$. (e) Results showing all the tracks found at time $t = 0$h within the reconstructed network.

The first step of particle tracking velocimetry was to record videos in the network using fluorescent microbeads tracers (Invitrogen FluoSpheres carboxylate 1.0 µm red 580/605 - added to the culture medium at a concentration of 6.7 µg/ml). In order to increase the signal to noise ratio, we excited the microbeads using the maximum intensity of the light source (Lumencor Sola light engine SM at 100%). The videos were recorded using a PCO Dimax at 400 fps and 2.5 ms exposure time. The recording was performed over ∼30 different positions to reconstruct the complete network (Fig 20a). Each video at each position was recorded during 75 ms. The videos were then analyzed using custom Matlab codes, which subtract the background to get rid of stacked beads, and then detect the particles position at every frame and reconstruct the trajectories from the position using the Hugarian optimization algorithm (Fig 20b). Once the trajectories were obtained, a filter was applied to get rid of short trajectories, and then, the velocity components at each point of each trajectory $i$ were computed as $v_x^i(t) = \frac{\Delta x^i(t)}{\Delta t}$ and $v_y^i(t) = \frac{\Delta y^i(t)}{\Delta t}$ (Fig 20c and Fig 20d). Next, another filter was applied to delete outliers and unphysical trajectories stemming from imaging noise. All videos, corresponding to different parts of the network, were then aligned to their corresponding spatial coordinates (Figure 20e) and a mask with a label for each channel was applied (same mask than in Fig 15a). In this way, every label contains the information for the velocities of all particles of a specific channel.

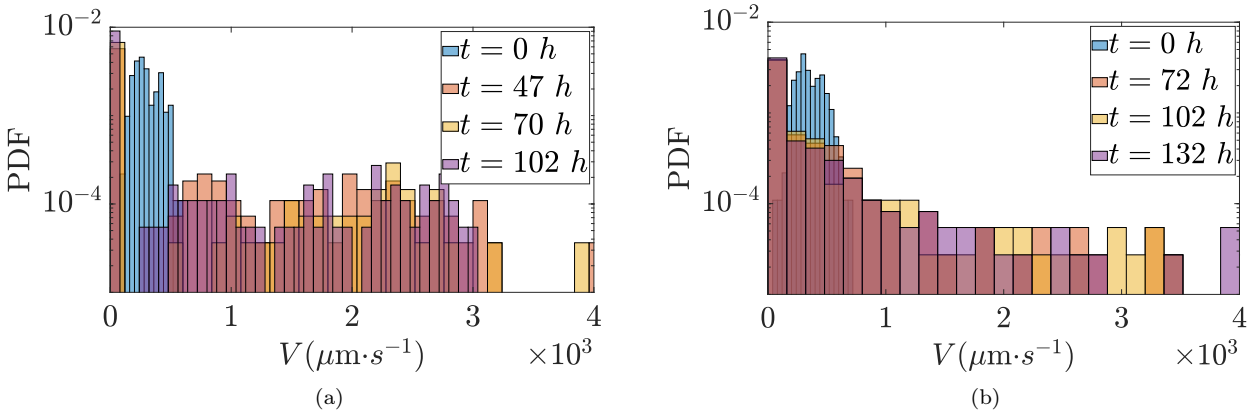
Once the velocities are assigned to each label, another filter is applied to delete very high velocities, in the event that salt-and-pepper noise yields to the detection of non-existing particles with large jumps that have spuriously large velocities. The limit velocity is $v_{lim} = 1.5 v_{max}$, where $v_{max}$ is the maximum possible value of the velocity profile at a flow rate of 2 µl/min. At time $t = 0$ h, we take $v_{max} = 740$ µm/s (empty channels, no biofilm colonization), and for the rest of the experiment, we consider an extreme case where the network has only two flow paths left, so as to obtain $v_{max} = 3700$ µm/s.

To obtain the velocities in the network, we finally average $v_x^i$ and $v_y^i$ for all particles $i$ within each channel (leading

to $\langle v_x \rangle$ and $\langle v_y \rangle$) and, for each channel $\alpha$ labeled from 1 to 229, the norm is calculated as $v_\alpha = \sqrt{\langle v_x \rangle_\alpha^2 + \langle v_y \rangle_\alpha^2}$. The result is then plotted using the graph functionalities of Matlab, with the colors and width of channels representing the velocity norm, e.g. in Fig 2 of the manuscript. The probability density function in the manuscript is the distribution of $v_\alpha$. Other examples for the distribution of $v_\alpha$ and the velocity representation on the network are shown in Figure 21 and Figure 22.

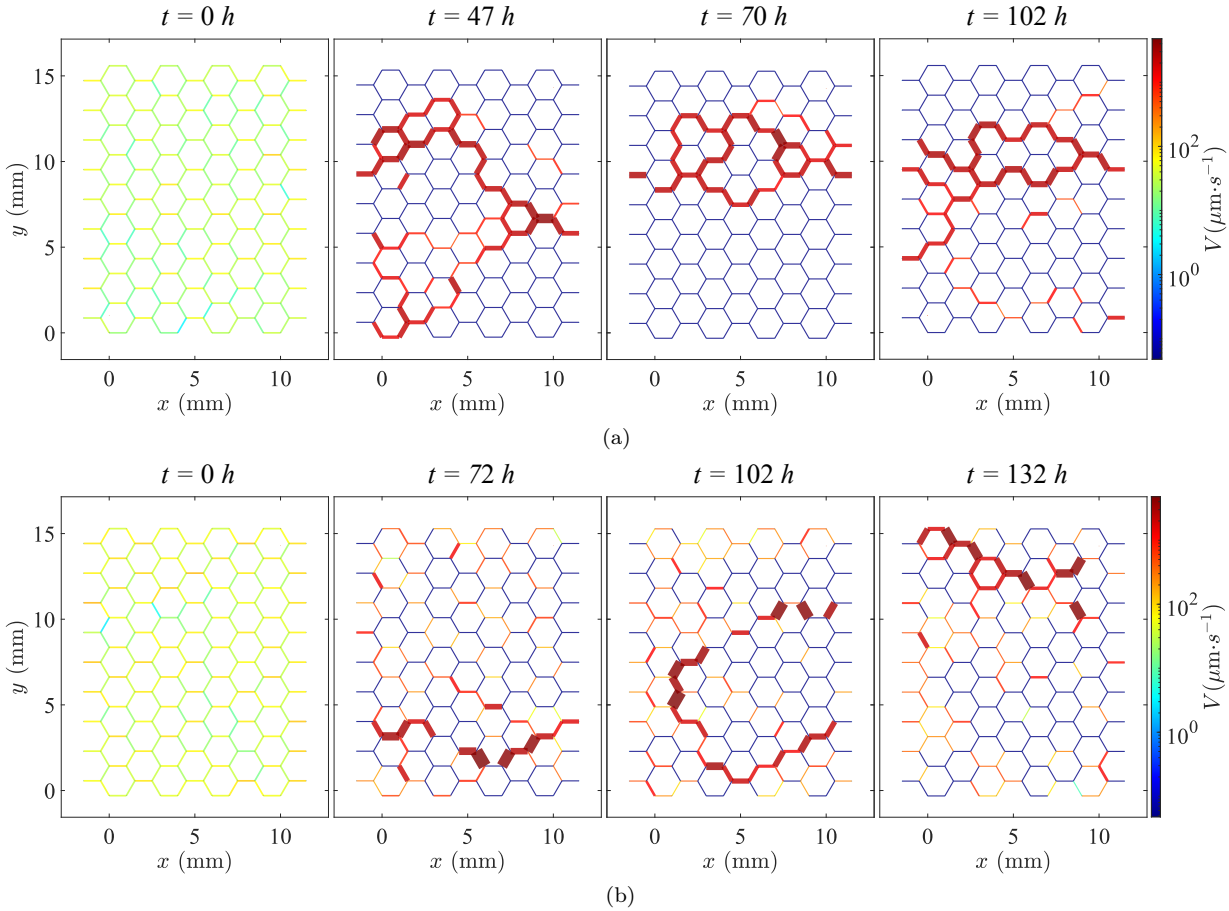
## B. PDF of velocity and preferential flow paths (PFPs) of replicates

1. PDF of velocity for triplicates at 2 µl/min




Supplementary figure 21: Triplicate: PDF of velocity for the two replicates shown here, at 2 µl/min, in addition to the replicate shown in the main text.

2. Preferential flow paths (PFPs) for triplicates at 2 µl/min




Supplementary figure 22: Triplicate: velocities within each channel at different times for the two replicates shown here, at 2 µl/min. We observe the creation of unstable preferential flow paths (PFPs) as shown in the replicate of the main text.